

Article

Performance and Modification Mechanism of Recycled Glass Fiber of Wind Turbine Blades and SBS Composite-Modified Asphalt

Yihua Nie *, Qing Liu, Zhiheng Xiang *, Shixiong Zhong and Xinyao Huang

School of Civil Engineering, Hunan University of Science and Technology, Xiangtan 411201, China; 15111103989@163.com (Q.L.); zsxnow@163.com (S.Z.); 15292276921@163.com (X.H.)

* Correspondence: nieyihua@hnust.edu.cn (Y.N.); mkl-jdx@163.com (Z.X.)

Abstract: Efficient disposal of composite materials recycled from wind turbine blades (WTB) at end-of-life needs to be solved urgently. To investigate the modification effects and mechanism on SBS-modified asphalt of the recycled glass fiber (GF) from WTB, GF-WTB/SBS composite-modified asphalt was prepared. Dynamic shear rheometer (DSR) and bending beam rheometer (BBR) were adopted to evaluate its performance. FTIR, SEM, EDS, and AFM methods were used to assess coupling agent pretreatment effects on GF-WTB and observe the modification mechanism. The macroscopic tests show that reasonable addition of GF-WTB effectively raises the high-temperature performance and low-temperature crack resistance evaluation index k -value of SBS-modified asphalt, and the optimal content is 2 wt% GF-WTB with 4 wt% SBS. FTIR, SEM, and EDS tests show GF-WTB can be successfully grafted by UP152 coupling agent and show that adhesion of the GF-WTB to the SBS-modified asphalt can be improved. AFM observation shows SBS and GF-WTB have good compatibility, improving the asphalt elasticity and toughness. This study provides a feasible solution for environmentally friendly regeneration of the composite materials from WTB and contributes to the development of the secondary modifier of SBS-modified asphalt.

Keywords: composite-modified asphalt; recycled glass fiber; wind turbine blades; silane coupling agent; SBS-modified asphalt



Citation: Nie, Y.; Liu, Q.; Xiang, Z.; Zhong, S.; Huang, X. Performance and Modification Mechanism of Recycled Glass Fiber of Wind Turbine Blades and SBS Composite-Modified Asphalt. *Appl. Sci.* **2023**, *13*, 6335. <https://doi.org/10.3390/app13106335>

Academic Editor: Luís Picado Santos

Received: 2 May 2023

Revised: 17 May 2023

Accepted: 20 May 2023

Published: 22 May 2023



Copyright: © 2023 by the authors. Licensee MDPI, Basel, Switzerland. This article is an open access article distributed under the terms and conditions of the Creative Commons Attribution (CC BY) license (<https://creativecommons.org/licenses/by/4.0/>).

1. Introduction

Wind power can offer clean and renewable energy with a low environmental impact and an increasing number of wind farms are built around the globe. The service life of a wind turbine blade (WTB) is typically 20–25 years [1]. However, many blades are coming out-of-service prior to that due to increasing power. The wind turbine industry is expected to store millions of tons of waste composite wind blades in the coming years [2–4]. These structures are mainly manufactured with glass fiber (with some use of carbon fiber) embedded in thermoset matrix materials such as epoxy, unsaturated polyester resin, or vinyl ester resins [5]. Waste disposal of fiber-reinforced polymer (FRP) composite materials from wind turbine blades at end-of-life, a majority of which are handled by landfills or incineration, is a problem that needs to be solved.

Due to the cross-linked structure after curing of the thermoset matrix materials, the thermoset composite cannot be melted and molded for the second time, meaning that the reinforced materials in thermoset composite are difficult to be recycled. Recycling technologies developed for thermoset composite materials mainly contain mechanical recycling, thermal recycling, and chemical recycling [6–8]. The latter two technologies are in the laboratory stage and currently have no practical application. Mechanical recycling is a simple physical process, which can partly recycle the reinforced materials in thermoset composite. Based on comparative analysis, the mechanical recycling seems to be the best choice at present. The mechanically recycled materials obtained by breaking up the

waste into particles or milling into fine powder are mainly used as fillers, reinforcement or raw materials for cement, concrete, etc. One of the most extensive research studies was carried out on Portland cement concrete in which mechanically recycled glass fiber-reinforced polymer (GFRP) waste was incorporated either as reinforcement, aggregate, or filler replacement [9,10]. Asokan et al. [11] assessed that GFRP waste substitution of fine aggregates in concrete could save approximately 15% of the fine aggregate cost. Presently, mechanical recycling has been applied in the waste composite recycling of WTB. Ribeiro et al. [12] reused the mechanically recycled GFRP pultrusion wastes from wind blades as aggregate and filler replacement for concrete–polymer composite materials. Schmidl and Hinrichs [13] mechanically recycled GFRP composites from blades which were used in cement production.

Rich studies have been carried out on various pristine fibers such as polymer fibers, lignin fibers, mineral fibers, glass fibers (GF), etc. in the application of asphalt pavement materials [14]. Many results indicate that the incorporation of fiber can significantly improve the high-temperature performance of asphalt. There are some applications of recycled fibers from waste fiber materials or thermoplastic materials such as waste plastic bottles added to asphalt pavement materials. However, few researchers reported the asphalt pavement engineering applications of recycled fibers from waste thermoset composites in wind energy, automotive, aerospace, construction industries, etc. Compared to the recycled fibers from waste fiber materials, the mechanically recycled glass fibers from wind turbine blades are of smaller size and blended with resin residues. By applying the recycled fibers from waste tires and waste plastic bottles or new polyester fiber to asphalt mixture, Liu [15] found that the high-temperature stability, water stability, and anti-fatigue properties were improved compared with ordinary asphalt mixtures; however, the effect was relatively insignificant compared with the new polyester fiber. Dehghan and Modarres [16] evaluated the effect of recycled polyethylene terephthalate (PET) fibers from waste plastic bottles on the fatigue properties of hot asphalt mix. Qilin Yang et al. [17] found recycled glass fiber chips from GFRP composite of waste airplane cabins blended into the 70/100 penetration bitumen improved high-temperature performance of the bitumen, water resistance, and low-temperature crack resistance of the bitumen mixture.

To summarize, mechanically recycled GF from WTB is viable and promising in the modification of the asphalt pavement materials and provides a new environmentally friendly recycling method for the waste WTB. Though mechanical recycling is relatively simple, the structure of the fiber may be damaged and the mechanical properties may be reduced in the recovery process. Considering the crushing, screening, and surface treatment process, the recycled GF from GFRP composites of WTB is the secondary modifier of SBS-modified asphalt in this study. Modifying the glass fiber prior to adding to SBS-modified asphalt can further improve the stability of composite-modified asphalt. These modification methods mainly include physical modification, surface chemical grafting, and surface chemical etching [18–24]. In this study, the surface chemical grafting by silane coupling agent was chosen as the surface treatment process. The objective of this study is to investigate the pretreated GF-WTB modification effects and mechanism on SBS-modified asphalt by macroscopic high- and low-temperature tests and microscopic observation, providing an effective regeneration solution for GFRP from waste WTB.

2. Materials and Experiments

2.1. Raw Materials and Sample Preparation

2.1.1. Matrix Asphalt and Raw GFRP Composites

The virgin asphalt binder in this study was AH-70 (60–80 penetration) from Petro-China Company Limited (Beijing, China). The raw glass fiber-reinforced polymer (GFRP) composites were obtained from the decommissioned wind turbine blade (WTB) at end-life, as seen in Figure 1a, which was crushed into small pieces using Los Angeles Abrasion Value machines by the Hunan Chuangyi Industrial Material Company (Xiangtan, China), as seen in Figure 1b.

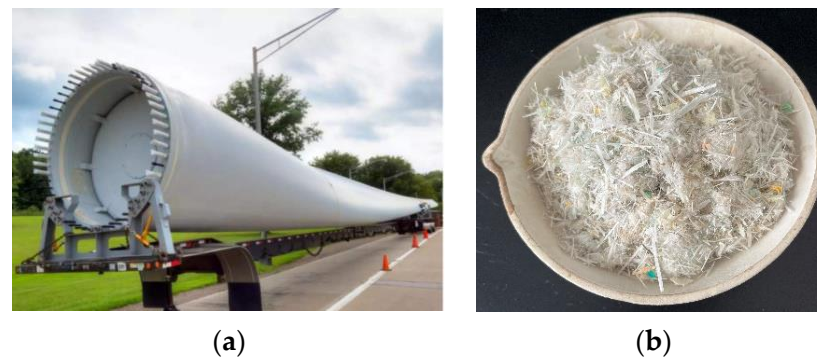


Figure 1. Raw GFRP composites from wind turbine blade at end-of-life: (a) wind turbine blade at end-of-life; (b) recycled GFRP.

2.1.2. Grading of GFRP Pieces

Using the vibrating screen machine (ZBSX-89), the raw GFRP pieces were screened and recycled with different diameters were mechanically separated. GF components were mainly distributed in the following several diameter particles: A (<0.075 mm), B (0.15–0.075 mm), C (0.3–0.15 mm), as seen in Figure 2. Among the three particle types, particle C is of the best degree of uniformity and relatively large size, which was selected as the original modifier in the following study.

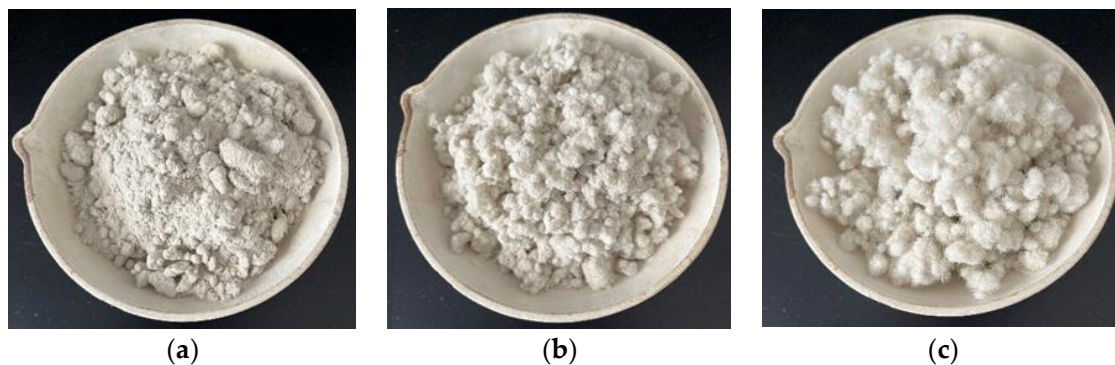


Figure 2. Three types of GF particles obtained after grading of GFRP pieces: (a) <0.075 mm; (b) 0.15–0.075 mm; (c) 0.3–0.15 mm.

2.1.3. GF Particles Heat- and Humidity-Resistance Check and Surface Treatment

According to current Chinese specification [25], under conditions of 210 °C and 1 h, the weight damage rate of the sample must be not more than 6% and the sample should not exhibit combustion. GF particles were placed in a beaker and heated in an oven at 210 °C for 1 h to measure the weight damage rate. With a mean damage rate of 3.2% from two measurements and no combustion, it was determined that the GF was resistant to high temperature and met the relative requirement for asphalt modification. For a humidity-resistance check, GF particles were prepared in a beaker with moderate deionized water and placed in a curing box at about 20 °C and 90% relative humidity to observe its shape and color changes and record quality change after 5 days. With no obvious change of color, no dispersed trend of the fiber clump, and a 1% (less than 5%) water absorption rate, it was determined that the GF was resistant to humidity and met the relative requirement for asphalt modification [25].

The GF particles surface treatment process was as follows. Firstly, the GF particles were dried at 230 °C for 1 h and after cooling they were then soaked in acetone for 1 h to remove the surface impurities. Three types of silane coupling agents (UP152, KH550, and KH792) were chosen for comparison. Silane coupling agent, ethanol, and water (at a volume ratio of 5:85:10) were stirred fully and the blend was placed for 10 min until

hydrolysis. The GF particles were immersed in quantitative coupling agent solution for 1 h and was then taken out to be dried and ready for use.

2.1.4. Preparation of GF-WTB/SBS-Modified Asphalt

Quantitative asphalt AH-70 was heated at 145 °C for 0.5 h to reach the flow state and evaporate water and then subsequently added with SBS (based on the weight of the matrix asphalt, 2, 3, 4, 5% SBS) and the blend was shear emulsified under 2000 rpm for 20 min at 160–170 °C.

Silane coupling agent modified GF-WTB was added to the prepared SBS-modified asphalt sample (based on the weight of the matrix asphalt, 0, 1, 2, 4% GF-WTB) and the GF-WTB was kept warm and swelled for 10 min at 160 °C. Then, the GF-WTB incorporated SBS-modified asphalt was evenly dispersed under 4000 rpm for 40 min at 140 °C and finally was developed for 10 min at 150 °C. The sample naming was shown in the following example. If the SBS modifier dosage was 2% and the GF-WTB dosage was 1%, the GF-WTB/SBS composite-modified asphalt sample was marked as SBS2 + WTB1. Figure 3 shows the preparation flowchart of the GF-WTB/SBS composite-modified asphalt.

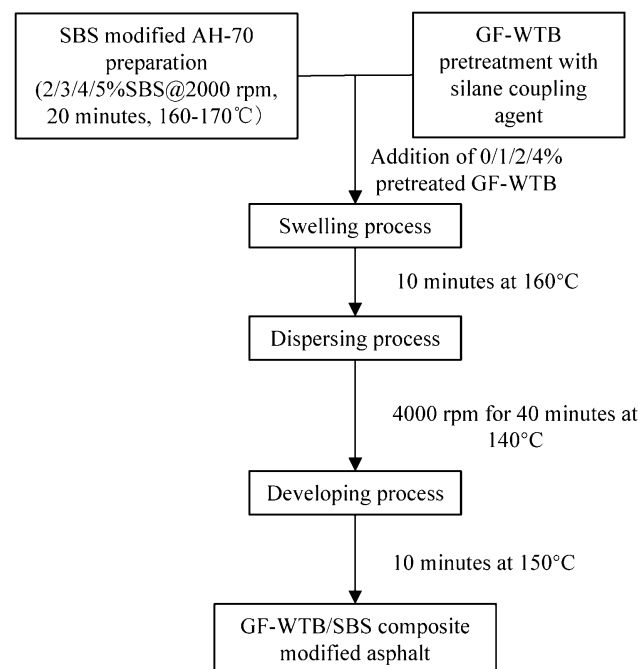


Figure 3. Flowchart of GF-WTB/SBS composite-modified asphalt preparation.

2.2. Rotational Viscosity

According to the standard test methods of asphalt for highway engineering [26], the rotational viscosity of the GF-WTB/SBS composite-modified asphalt was tested using a Brookfield viscometer (model NDJ-1F, Shanghai Changji Geological Instrument Co., Ltd, Shanghai, China) at 135 °C.

2.3. Dynamic Shear Rheometer (DSR) Test

The DSR test was used to characterize viscous and elastic behavior of the GF-WTB/SBS composite-modified asphalt at medium to high temperatures. The DSR model used in the test was DHR-3, adopting the sinusoidal strain control mode. The gap and the diameter for the test were 1 mm and 25 mm, respectively. The angular velocity was 10 rad/s, the control strain was 12%, the range of the scanning temperature was 40–76 °C, and the heating rate was 2 °C/min. For each experimental run using the DSR test, two replicate specimens were measured to avoid the wrong operation or a sample preparation deviation.

2.4. Bending Beam Rheometer (BBR) Test

The BBR test provided a measurement of low-temperature stiffness and relaxation properties of the GF-WTB/SBS composite-modified asphalt. In order to obtain the test results in a relatively short time, according to the time-temperature equivalence principle [27], SHRP researchers increased the test temperature by 10 °C, and the same creep stiffness S-value and the stiffness change rate m-value were obtained when the sample was loaded for 60 s. According to the specification AASHTO T313-2012 [28], the heated sample was poured into BBR mold and after cooling and demolding the asphalt beam was placed in the BBR bath at test temperature for 60 min. In this study, test temperatures of −12 °C, −18 °C, and −24 °C were set and all stiffnesses and m-values were the mean of three measurements.

2.5. Fourier Transform Infrared Spectroscopy (FTIR) Test

Infrared spectral analysis is one of the most widely used methods in the study of chemical structure of polymers. In this study, by comparing with the untreated GF particles and observing the changes in the absorption peaks of the main functional groups, characteristics of the functional groups in silane coupling agent pretreated GF particles were expected to be obtained and the surface treatment process of GF particles was expected to be further understood based on chemical changes. The FTIR (Thermo Scientific Nicolet 6700, Waltham, MA, USA) parameters were revolution 4 cm^{−1} with a scan number of 32 times. The sample was blended with potassium bromide (KBr) with ratio of about 1:10, grinded fully, and finally tableted to thin circularity chip. Immediately, the prepared circular specimen was put into FTIR and scanned by infrared light. To avoid the wrong operation or a sample preparation deviation, for each experimental run using the FTIR test, two parallel specimens were measured.

2.6. Scanning Electron Microscope (SEM) Observation and Energy Dispersive Spectrometer (EDS) Analysis

SEM (Zeiss sigma 300) photographs were obtained to observe the surface morphology changes of silane coupling agent pretreated GF particles compared to the untreated GF particles. The SEM accelerating voltage was 15 kV and the imaging probe was SE2. The sample was scattered on the conductive glue stuck on the sample stage, sprayed with a thin layer of gold, and then put into the SEM for observation. Combined with the surface morphology observation, the elements distribution on the silane coupling agent pretreated GF particle sample surface was obtained by using the scanning function of the EDS equipped on the SEM.

2.7. Atomic Force Microscope (AFM)

AFM was used to examine the morphology of the matrix asphalt, SBS-modified asphalt, and GF-WTB/SBS composite-modified asphalt at the nanoscale. The asphalt sample was heated and dropped onto the microscope slide to shape the thin film. After cooling down, the AFM specimen was tested by Bruker Dimension ICON in tapping mode.

3. Results and Discussion

The basic technical properties of the virgin asphalt binder AH-70 are listed in Table 1.

Table 1. Technical properties of AH-70.

Technical Index	Specification Requirement	Test Result	Experimental Method [26]
Penetration@25 °C, 100 g, 5 s (0.1 mm)	60~80	60.3	T0604
Penetration index (PI)	−1.5~1.0	−0.5	T0604
Ductility@15 °C, 5 cm/min (cm)	≥100	>120	T0605
Softening point (°C)	≥45	47	T0606

Table 1. Cont.

Technical Index		Specification Requirement	Test Result	Experimental Method [26]
Rotational viscosity@135 °C (Pa·s)		-	0.571	T0625
Mass change (%)		$\leq \pm 0.8$	0.1	T0610
RTFOT residue	Residual penetration ratio (%)	≥ 61	65	T0604
	Residual ductility @15 °C (cm)	≥ 15	21.8	T0605

3.1. Rotational Viscosity

The effect of GF-WTB content on the rotational viscosity of a certain content (2, 3, 4, or 5 wt%) SBS-modified binders is shown in Figure 4. Figure 4 is the average of the measurement results. Three specimens of each asphalt were measured to ensure reliable test results. The maximum coefficient of variation (CV) of each asphalt sample group in the rotational viscosity test was 3.5%. As seen in Figure 4, the rotational viscosity values of a certain content SBS-modified binders increase with the GF-WTB content. The values of the 5 wt% SBS-modified binder ranged from 3.5 Pa·s for 0 wt% GF-WTB content to 3.9 Pa·s for 4 wt% content, which are both larger than 3.0 Pa·s, which is the maximum allowable value in SHRP specification considering mixing performance. Therefore, the 5 wt% SBS-modified binder was only used for the trend evaluation in the following analysis. In the figure, the maximum rotational viscosity increasing rate 17% appeared in the 4 wt% SBS-modified binder from 2.3 Pa·s for 1 wt% GF-WTB content to 2.7 Pa·s for 2 wt% content. The rotational viscosity test results will be helpful to further research for GF-WTB/SBS composite-modified asphalt mixture pavement performance.

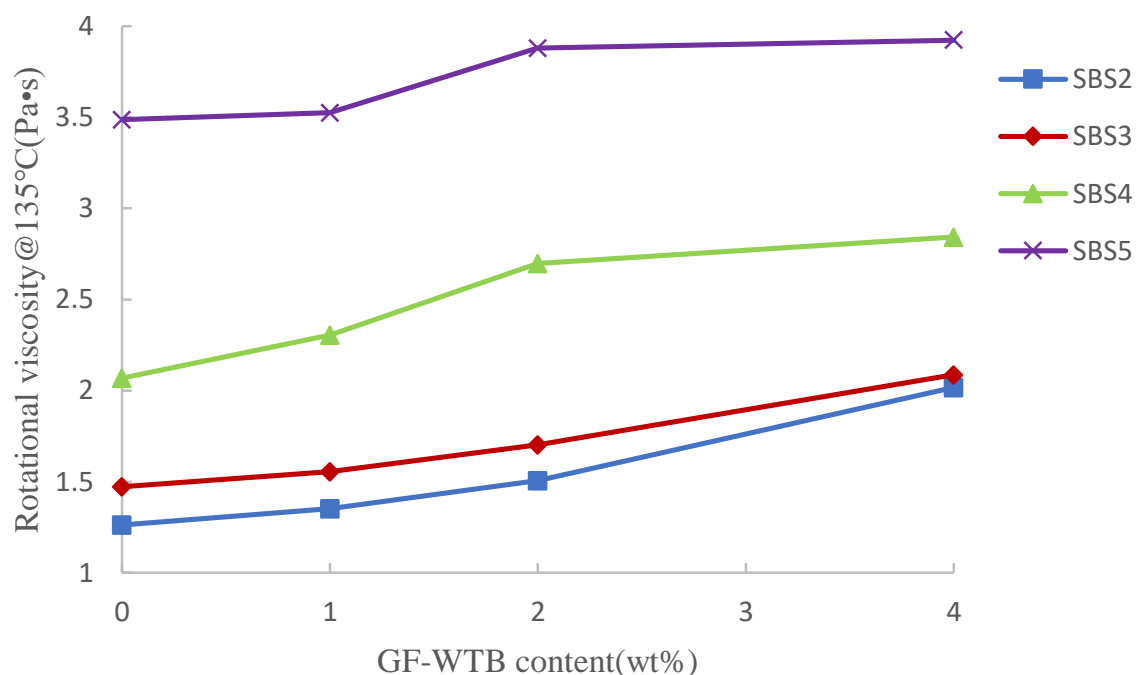
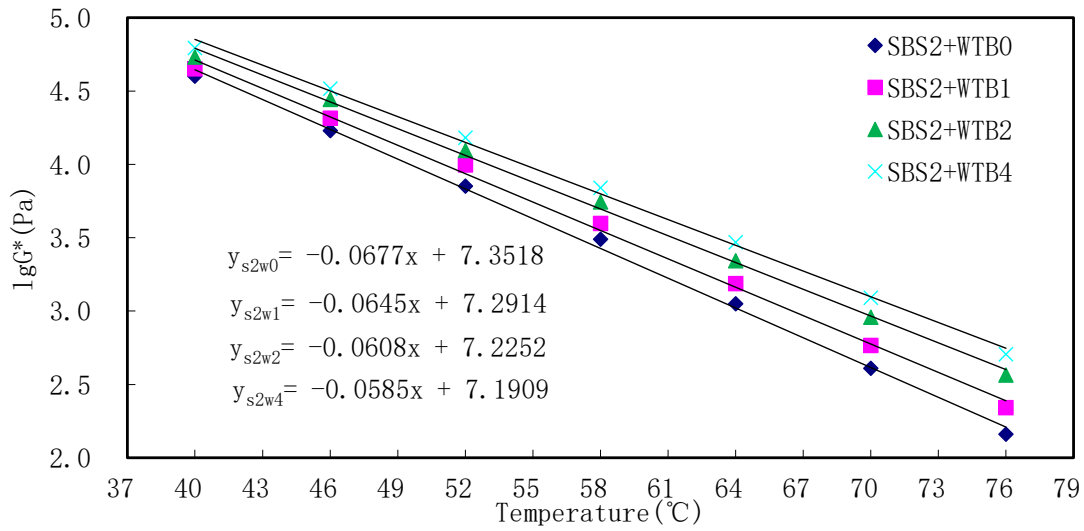


Figure 4. Effect of GF-WTB content on rotational viscosity under certain SBS dosage.

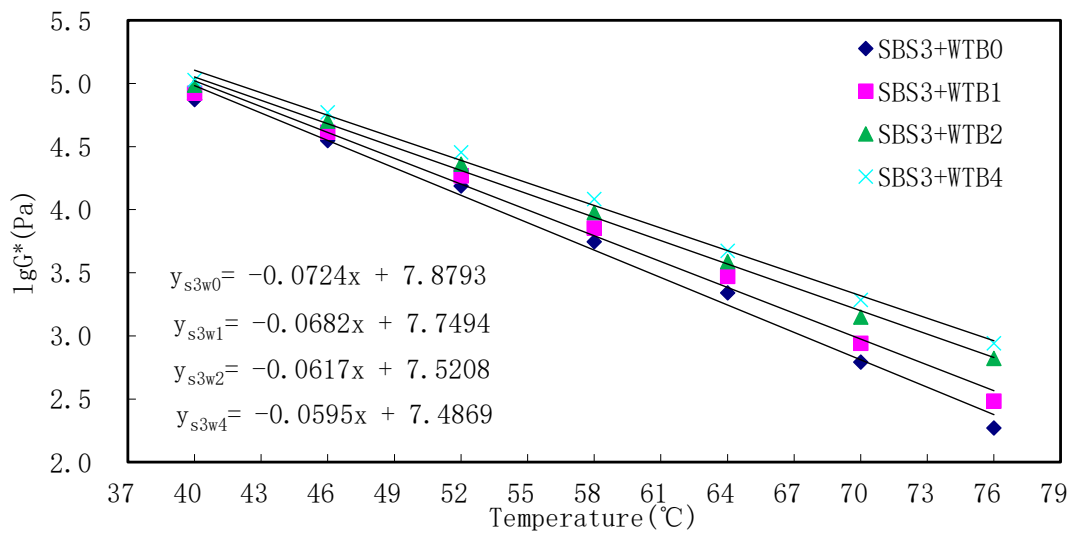
3.2. Dynamic Rheological Properties and Temperature Sensitivity

The complex shear modulus G^* can be considered the binder sample's total resistance to deformation when repeatedly sheared. The $\log G^*$ values of the 2, 3, 4, or 5 wt% SBS-modified binders with different GF-WTB contents vs. temperatures from 40 °C to 76 °C are shown in Figure 5. Figure 5 shows that the $\log G^*$ values linearly decrease with the increase in temperature for all the asphalt samples. For the same SBS content, the $\log G^*$ value at the end temperature 76 °C increases obviously with the GF-WTB content. In addition,

the sensitivity of $\log G^*$ to temperature, i.e., the regression coefficient (regression line slope), decreases with the increase in GF-WTB dosage under certain SBS content. The DSR test result analysis indicates that the addition of silane coupling agent modified GF-WTB reduces G^* temperature sensitivity of the SBS-modified asphalt and the increase in the G^* value of binder will transmit to the increase in the stiffness of respective asphalt mixture.

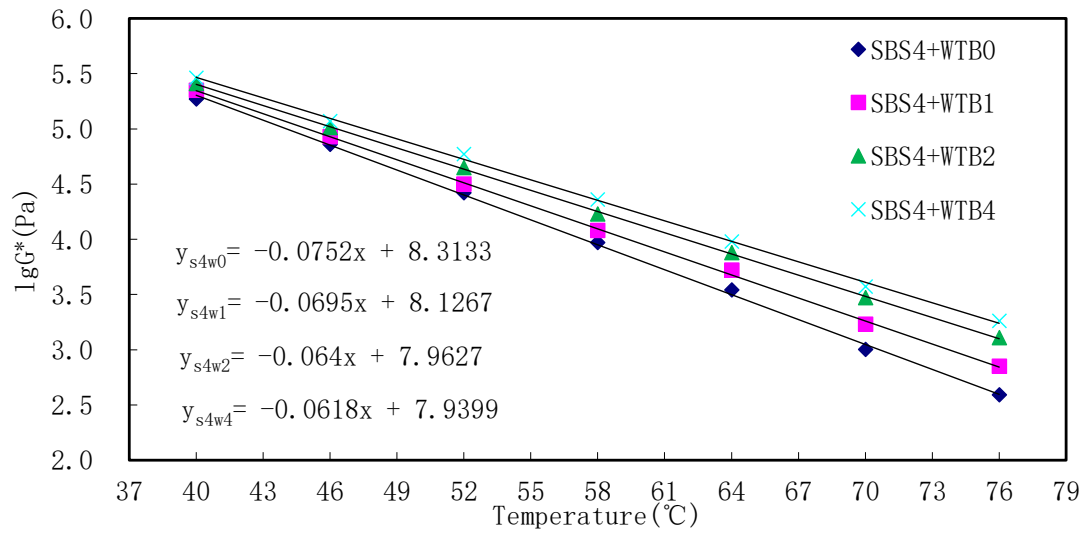


(a)

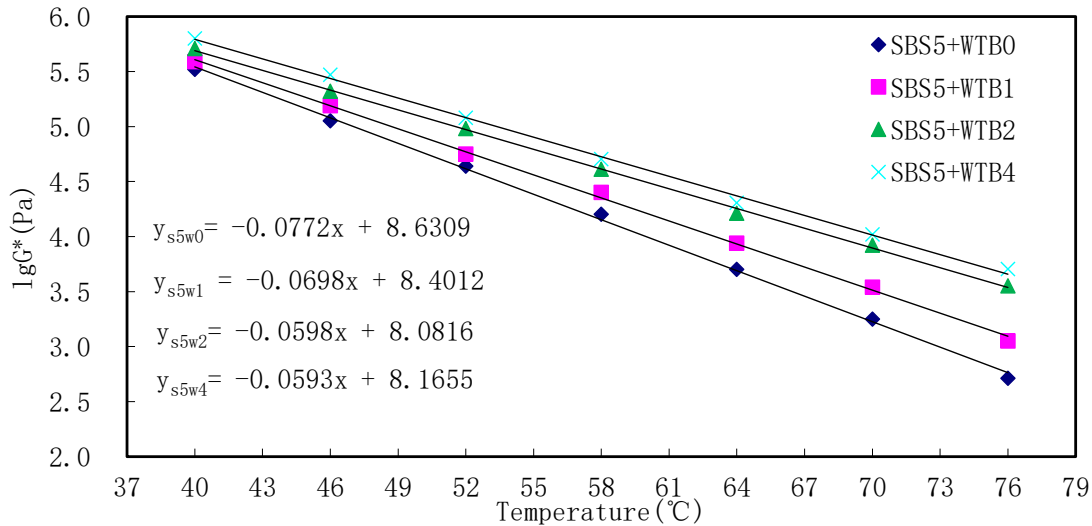


(b)

Figure 5. Cont.



(c)

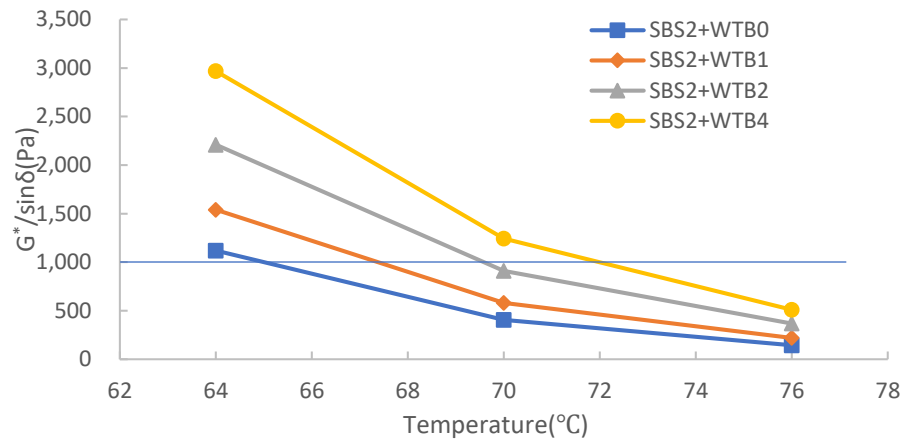


(d)

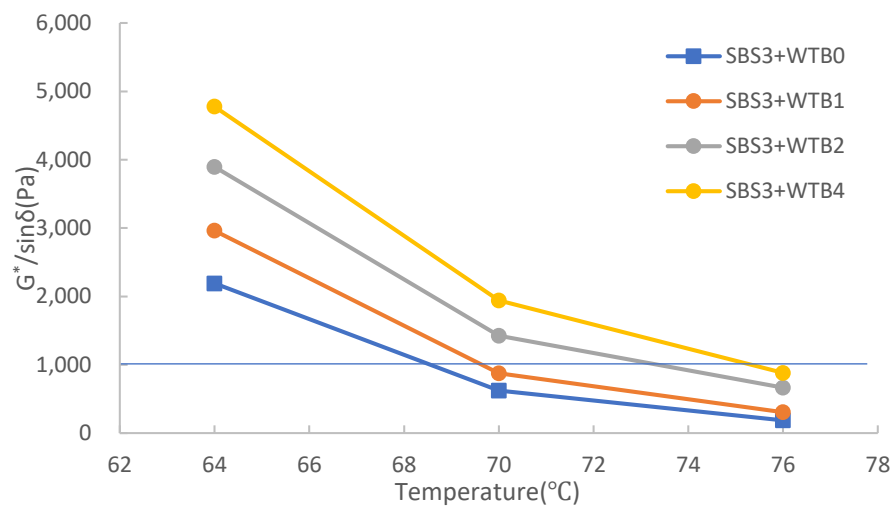
Figure 5. The logarithm of the complex shear modulus of GF-WTB/SBS composite-modified asphalt: (a) SBS2 + WTBx; (b) SBS3 + WTBx; (c) SBS4 + WTBx; (d) SBS5 + WTBx.

Under the same G^* value, the smaller the phase angle δ , which means the large elastic component and the small viscous one, the stronger the anti-rutting ability of the asphalt material. Under high-temperature conditions, the larger $G^*/\sin \delta$ indicates that G^* is larger and δ is smaller [29]. Therefore, the rutting factor $G^*/\sin \delta$ is used to represent the anti-rutting ability in the SHRP specification. The $G^*/\sin \delta$ values of the 2, 3, 4, or 5 wt% SBS-modified binders with different GF-WTB contents vs. high temperatures 64–76 °C are shown in Figure 6. The Figure 6 shows that the $G^*/\sin \delta$ values decrease with the increase in high temperature for all the asphalt samples. Evidently, the rutting factor increases with the SBS dosage. The horizontal line in Figure 6 represents the minimum $G^*/\sin \delta$ value 1.0 kPa for the unaged binder in the performance-graded DSR specifications. Under the same SBS content, the addition of silane coupling agent modified GF-WTB improves the high-temperature performance grade, e.g., for 4 wt% SBS-modified asphalt, incorporation of 2 or 4 wt% GF-WTB elevates the high-temperature PG from 70 °C to 76 °C. The DSR test results show that GF-WTB/SBS composite-modified binders are of better resistance to deformation, anti-rutting ability, and temperature-insensitivity. Among the

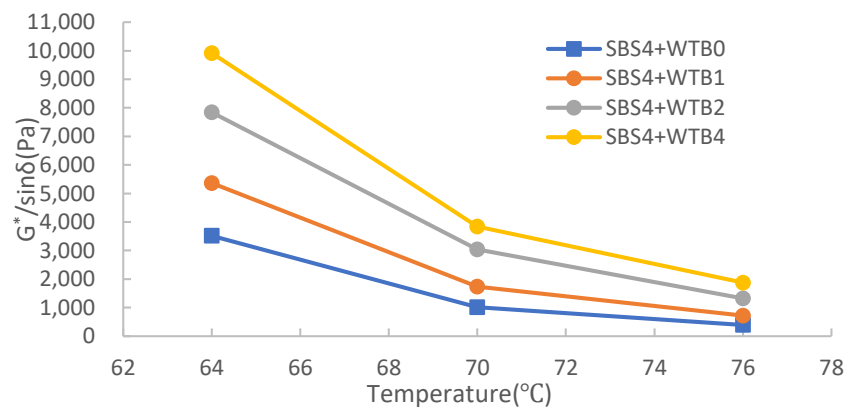
composite-modified binders with 2, 3, 4 wt% SBS, in comprehensively considering the high-temperature PG, temperature sensitivity, and GF-WTB dosage, SBS4 + WT B2 is the optimal one.



(a)

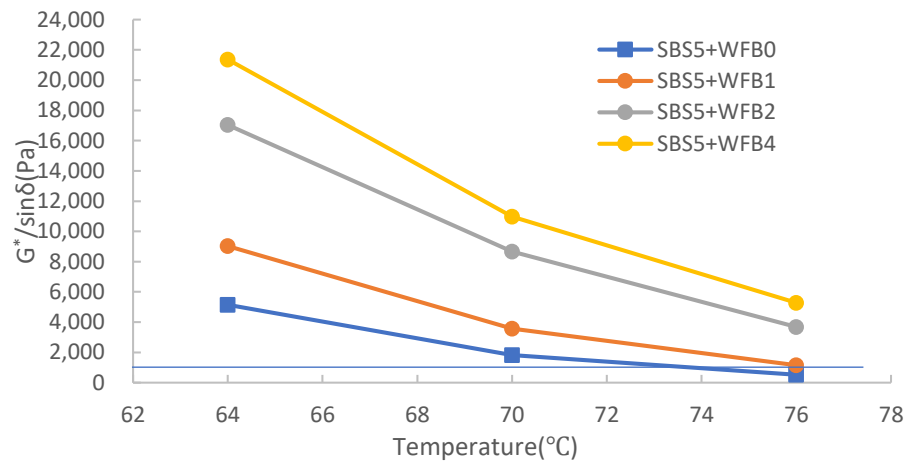


(b)



(c)

Figure 6. Cont.



(d)

Figure 6. The rutting factor and high-temperature PG of GF-WTB/SBS composite-modified asphalt: (a) SBS2 + WTbX; (b) SBS3 + WTbX; (c) SBS4 + WTbX; (d) SBS5 + WTbX.

3.3. Low-Temperature Properties

In this study, BBR test temperatures of $-12\text{ }^{\circ}\text{C}$, $-18\text{ }^{\circ}\text{C}$, and $-24\text{ }^{\circ}\text{C}$ were set and S-values and m-values of all GF-WTB/SBS composite-modified binders are in Tables 2 and 3. Tables 2 and 3 present the average of the measurement results. Three BBR specimens of each asphalt were measured to ensure reliable test results. The maximum coefficient of variation of each asphalt sample group in the BBR test was 5.0%. Table 2 shows under $-12\text{ }^{\circ}\text{C}$ and 60 s loading conditions, with S-values and m-values of four SBS2 + WTb binders and four SBS3 + WTb binders all satisfying $S \leq 300\text{ MPa}$ and $m \geq 0.3$ SHRP specification demands, respectively, and meeting performance-grade PG-22. In addition, for SBS3 + WTb1 and SBS3 + WTb4, the performance grades also reached PG-28 demand. Table 3 shows four SBS4 + WTb binders and four SBS5 + WTb binders that can meet performance-grade PG-34.

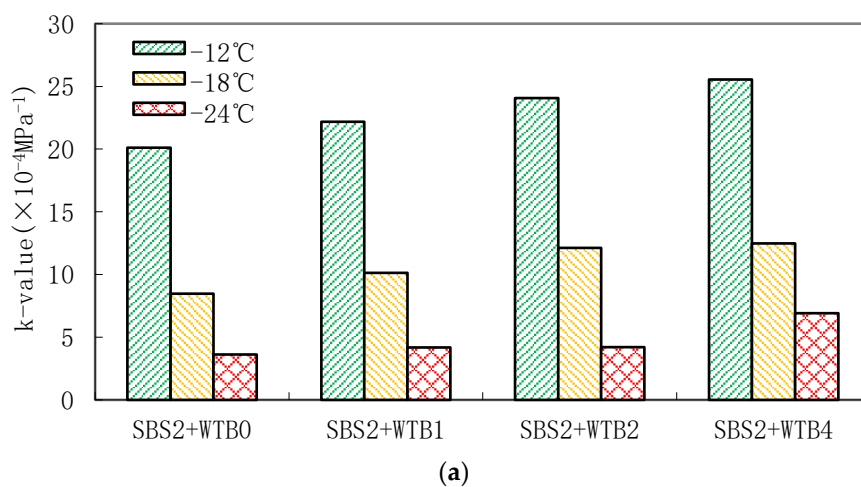
Table 2. BBR test results of SBS2 + WTbX and SBS3 + WTbX.

Temp (°C)	Index of BBR Test	Code of the Asphalt Binder							
		SBS2 + WTb0	SBS2 + WTb1	SBS2 + WTb2	SBS2 + WTb4	SBS3 + WTb0	SBS3 + WTb1	SBS3 + WTb2	SBS3 + WTb4
-12	S (MPa)	175	142	160	121	121	112	106	115
	m	0.352	0.315	0.385	0.309	0.312	0.306	0.294	0.321
	k ($\times 10^{-4}\text{ MPa}^{-1}$)	20.11	22.18	24.06	25.54	25.79	27.32	27.74	27.91
-18	S (MPa)	368	303	208	209	187	198	171	167
	m	0.312	0.307	0.252	0.261	0.279	0.301	0.292	0.305
	k ($\times 10^{-4}\text{ MPa}^{-1}$)	8.48	10.13	12.12	12.49	14.92	15.20	17.07	18.26
-24	S (MPa)	661	615	594	375	391	340	302	281
	m	0.240	0.257	0.250	0.259	0.273	0.265	0.290	0.295
	k ($\times 10^{-4}\text{ MPa}^{-1}$)	3.63	4.18	4.21	6.91	6.98	7.79	9.60	10.50
	Performance grade	PG-22	PG-22	PG-22	PG-22	PG-22	PG-28	PG-22	PG-28

Table 3. BBR test results of SBS4 + WTBx and SBS5 + WTBx.

Temp (°C)	Index of BBR Test	Code of the Asphalt Binder							
		SBS4 + WTB0	SBS4 + WTB1	SBS4 + WTB2	SBS4 + WTB4	SBS5 + WTB0	SBS5 + WTB1	SBS5 + WTB2	SBS5 + WTB4
−12	S (MPa)	116	107	106	103	96	93	91	89
	m	0.343	0.323	0.342	0.347	0.339	0.341	0.346	0.344
	k ($\times 10^{-4}$ MPa $^{-1}$)	29.57	30.19	32.26	33.69	35.31	36.67	38.02	38.65
−18	S (MPa)	145	140	132	128	119	115	111	108
	m	0.312	0.317	0.330	0.338	0.332	0.337	0.342	0.339
	k ($\times 10^{-4}$ MPa $^{-1}$)	21.52	22.64	25.00	26.41	27.90	29.30	30.81	31.39
−24	S (MPa)	263	256	231	246	220	223	184	186
	m	0.306	0.311	0.302	0.331	0.325	0.333	0.301	0.313
	k ($\times 10^{-4}$ MPa $^{-1}$)	11.63	12.15	13.07	13.46	14.77	14.93	16.36	16.83
	Performance grade	PG-34	PG-34	PG-34	PG-34	PG-34	PG-34	PG-34	PG-34

Relative research shows that when the low-temperature grade of PG classification is set every 6 °C, although different asphalts under the same PG low-temperature grade have the same classification standard, the difference in low-temperature performance between them cannot be reflected [30,31]. Based on the S and m indexes, a new low-temperature evaluation index $k = m/S$ is proposed by combining the two together; that is, the creep rate of asphalt under the unit creep stiffness. It can be seen from the representation that the larger the k index, meaning small creep stiffness and large stiffness change rate, the better the low-temperature crack resistance of asphalt. The index k-values under −12 °C, −18 °C, or −24 °C vs. GF-WTB contents of certain SBS dosage-modified asphalt are shown in Figure 7 and the k-values data are in Tables 2 and 3. Figure 7 shows that k-values decrease with the test temperature decreasing for all the asphalt samples and k-value increases evidently with the SBS dosage increasing. Under the same SBS dosage, GF-WTB content elevates the k-value and the low-temperature crack resistance of SBS-modified asphalt. For SBS4 + WTB composite-modified binders under −12 °C, −18 °C, or −24 °C, from 0 to 4 wt% GF-WTB k-value increases by 13.9%, 22.7%, 15.7%, respectively, from 1 to 2 wt% GF-WTB by 6.9%, 10.4%, 7.5%, respectively, and from 2 to 4 wt% GF-WTB only by 4.4%, 5.6%, 3%, respectively. In comprehensively considering the k-value increasing rate and GF-WTB dosage, SBS4 + WTB2 is the optimal combination.

**Figure 7.** Cont.

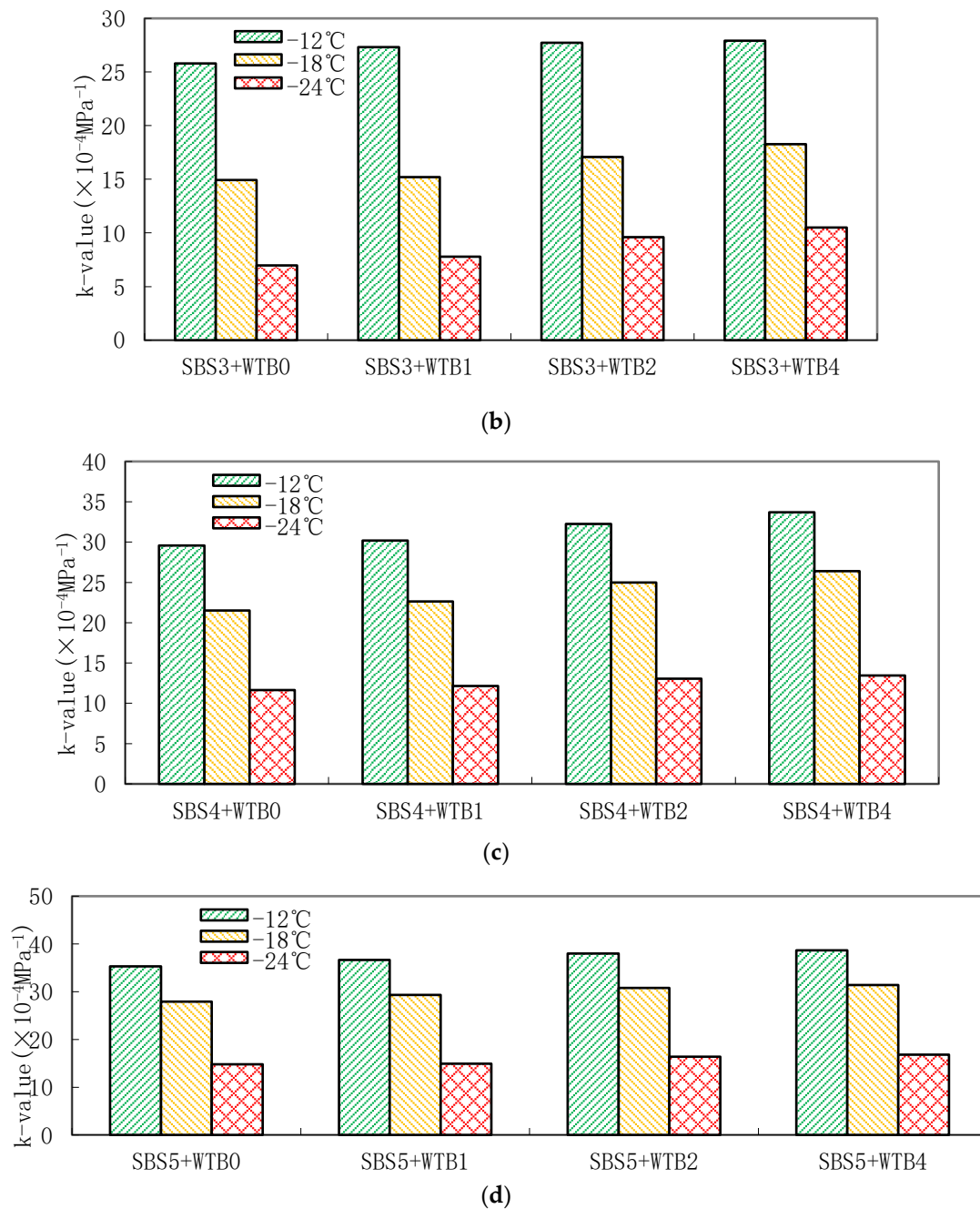


Figure 7. Effect of GF-WTB content on BBR k-value under certain SBS dosage and temperature: (a) SBS2 + WTBy; (b) SBS3 + WTBy; (c) SBS4 + WTBy; (d) SBS5 + WTBy.

3.4. Fourier Transform Infrared Spectroscopy (FTIR) Test

The silane coupling agent UP152 used in the study with the chemical name vinyltriacetoxysilane and the molecular formula $C_8H_{12}O_6Si$ was produced by the Nanjing Upchemical company. The chemical reaction mechanism between GF-WTB and UP152 is shown in Figure 8. The UP152 Si functional groups acetoxy -OAc hydrolyze and generate silanol Si-OH, which are unsteady and generate Si-O-Si in further polycondensation, and the carbon functional group vinyl $CH_2=HC-$ in UP152 can react with some organic functional groups in asphalt materials. Therefore, the UP152 can couple the inorganic glass fiber recycled from WTBy with the organic asphalt materials.

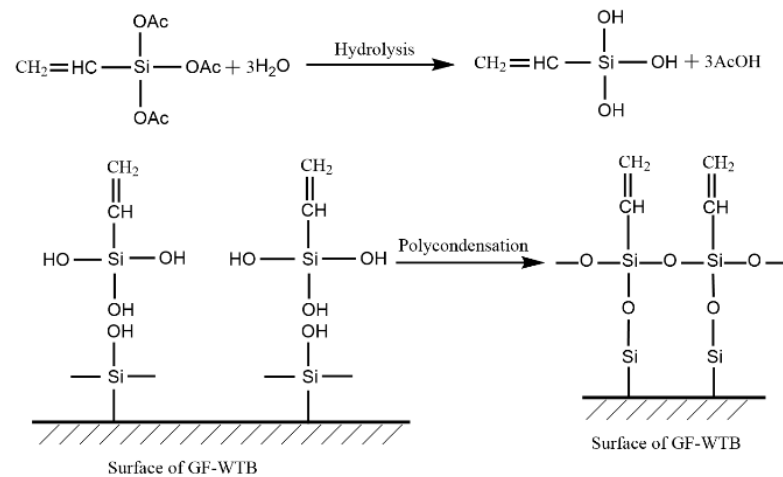


Figure 8. Chemical reaction mechanism between GF-WTB and UP152.

The FTIR spectrograms of the untreated GF-WTB and UP152-modified GF-WTB are in Figure 9. Absorption peaks at 2929 and 2872 cm^{-1} for the original GF-WTB respectively represent C-H stretching of CH_2 and CH in aliphatic of the polyester resin curing agent residues, corresponding to 2954 and 2842 cm^{-1} for the modified GF-WTB [32]. The original GF-WTB and the UP152-modified GF-WTB show the band corresponding to the C=O stretching of the polyester resin curing agent residues respectively at 1728 cm^{-1} and 1720 cm^{-1} [33]. The new absorption peaks at 1635 and 1454 cm^{-1} for UP152-modified GF-WTB respectively characterize the carbon functional group vinyl C=C stretching and the vinyl CH_2 scissor bending vibration. Absorption peaks at 1091, 699, and 479 cm^{-1} for the modified GF-WTB characterize the antisymmetric stretching, symmetric stretching, and bending vibration of Si-O-Si, with the corresponding bands 1073, 699, and 477 cm^{-1} for the original GF-WTB. The three absorption peaks all show the same trend; that is, the absorption peak of UP152-modified GF-WTB is stronger than that of original one. It shows that the chemical reaction between the coupling agent and the glass fiber surface produces new Si-O-Si bonds. The analysis of the FTIR results shows that the silicon coupling agent UP152 was successfully grafted to the surface of the recycled glass fiber from WTb.

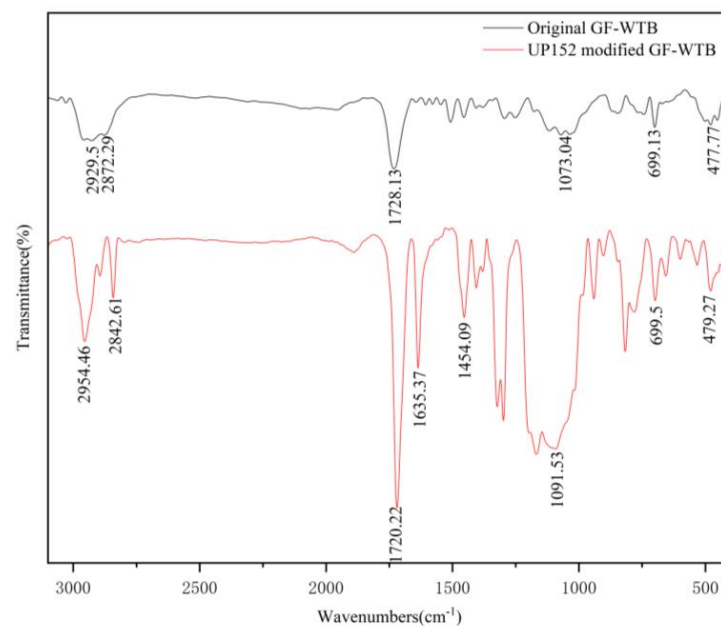


Figure 9. FTIR spectrograms of untreated GF-WTB and UP152-modified GF-WTB.

3.5. Scanning Electron Microscope (SEM) Observation and Energy Dispersive Spectrometer (EDS) Analysis

The SEM photographs of the untreated GF-WTB and UP152-modified GF-WTB are shown in Figure 10. It can be seen from the figure that the surface of the original GF-WTB is smooth without any rough groove structure except for some resin curing agent residues scattered on it. After the modification of UP152, the surface of the fiber is covered with a rough graft layer of silane coupling agent and the fiber diameter also increases, indicating that the graft layer of the coupling agent UP152 has a certain thickness. Figure 11 shows the corresponding EDS element spectrum by spot scanning, and relative contents of elements are listed in Tables 4 and 5. Tables 4 and 5 show that after UP152 modification, the C element on the surface of GF-WTB increases significantly, Si and O contents decrease, and Ca element decreases significantly, indicating that the coupling agent UP152 was successfully grafted.

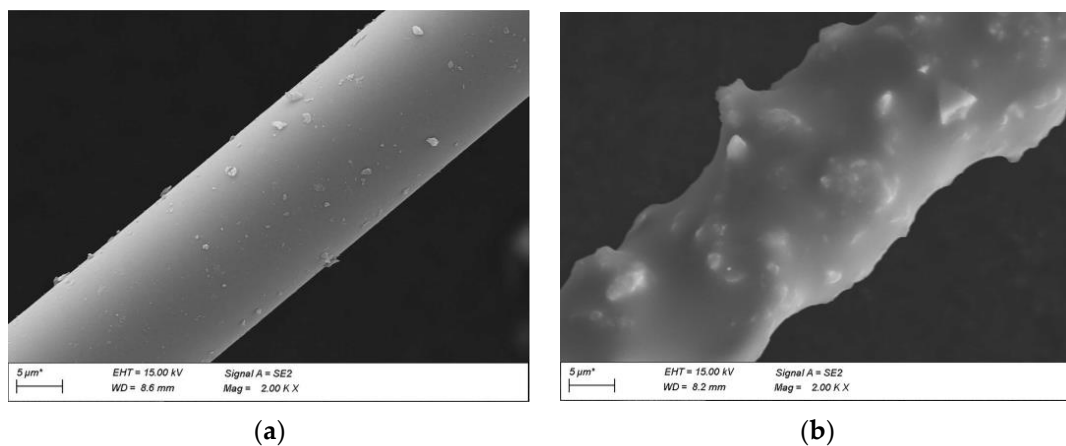


Figure 10. SEM photographs of the GF-WTB: (a) untreated; (b) UP152-modified.

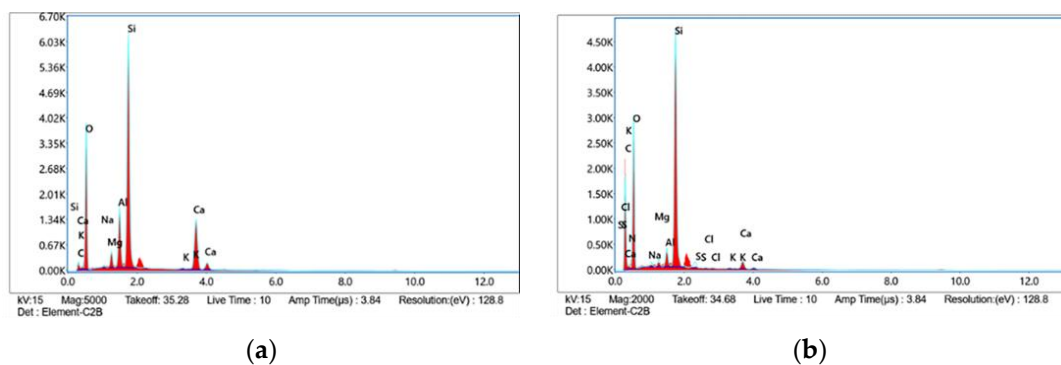


Figure 11. EDS element spectrum of the GF-WTB: (a) untreated; (b) UP152-modified.

Table 4. Element content of untreated GF-WTB.

Element	Series	Weight %	Atomic %	Error %
C	K	0.36	0.67	20.36
O	K	38.94	54.84	9.30
Na	K	0.45	0.44	14.88
Mg	K	2.08	1.92	7.38
Al	K	7.61	6.36	4.74
Si	K	30.53	24.50	3.72
K	K	0.36	0.21	17.17
Ca	K	19.67	11.06	3.19

Table 5. Element content of UP152-modified GF-WTB.

Element	Series	Weight %	Atomic %	Error %
C	K	33.31	45.25	10.20
N	K	2.27	2.65	20.96
O	K	34.26	34.94	9.54
Na	K	0.66	0.47	17.17
Mg	K	0.71	0.48	12.25
Al	K	1.82	1.10	6.57
Si	K	23.20	13.48	3.05
S	K	0.86	0.44	14.94
Cl	K	0.11	0.05	23.64
K	K	0.28	0.12	13.49
Ca	K	2.52	1.03	7.85

According to the FTIR, SEM, and EDS analysis of the UP152-modified GF-WTB, the coupling agent grafted fiber surface becomes thicker and rougher and introduces a vinyl functional group, which improves the adhesion of the grafted GF-WTB to the SBS-modified asphalt.

3.6. Atomic Force Microscope (AFM)

Figure 12a–c show the AFM three-dimensional images of the matrix asphalt, SBS-modified asphalt (with 4 wt% SBS), and GF-WTB/SBS composite-modified asphalt (with 4 wt% SBS and 2 wt% GF-WTB), respectively. In Figure 12, the dark areas are pits and the bright areas are bumps. It can be seen from Figure 12a that the microscopic morphology of the matrix asphalt surface is relatively uniform. The surface is distributed with alternating dark and pale areas, which are close to bee-shaped structure. Research shows that these bee-shaped structures are the clustering of the asphaltene micelles not completely dispersed in the dispersion medium [34]. It can be seen from Figure 12b that the surface of SBS-modified asphalt presents a network structure, which is formed by the SBS block copolymer crosslink and swelling by absorbing light components in asphalt. This network structure can effectively change the elasticity, plasticity, and ductility of asphalt, thereby improving the high- and low-temperature performance of asphalt.

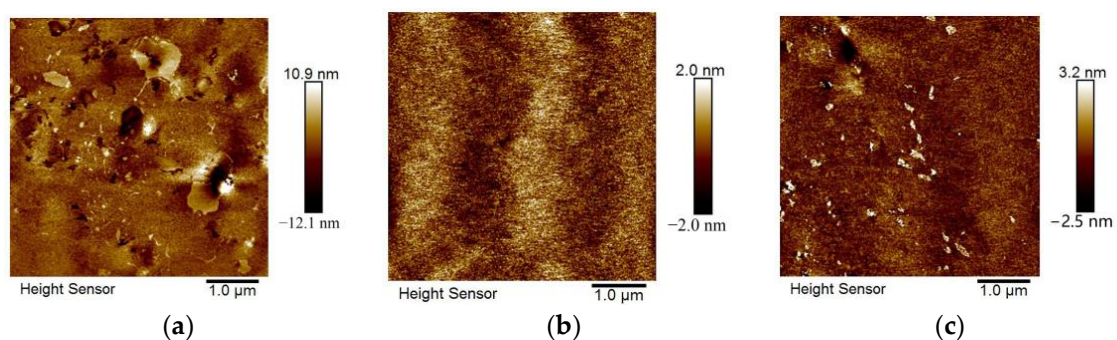


Figure 12. AFM of: (a) matrix asphalt; (b) SBS-modified asphalt; (c) GF-WTB/SBS composite-modified asphalt.

From Figure 12c, the convex GF-WTB particles (white areas) can be clearly seen in the SBS-modified asphalt network structure, and the two modifiers have good compatibility. During preparation, the GF-WTB/SBS composite-modified asphalt was stirred and developed at a high temperature. Swelling, adsorption of the asphalt light components, and reaction between some organic functional groups in asphalt and the vinyl functional group on grafted GF-WTB particles surface occurred. Then, the GF-WTB agents were evenly dispersed in the SBS-modified asphalt in the form of particles and chains, and the

GF-WTB/SBS composite-modified asphalt obtained better toughness and low-temperature crack resistance.

4. Conclusions

In this study, composite-modified asphalt composed of silane coupling agent pretreated recycled GF from WTB and SBS-modified asphalt was investigated in terms of modification effects and mechanism. The following conclusions can be drawn from this research:

- (1) The recycled GF particles from WTB are of good heat- and humidity-resistance performance and in regular asphalt performance tests the rotational viscosity of SBS-modified binders evidently increases with the GF-WTB addition dosage under certain SBS content. In the high-temperature rheology performance DSR test, GF-WTB/SBS composite-modified binders presented better resistance to deformation, anti-rutting ability, and temperature-insensitivity.
- (2) In the low-temperature BBR test, for 4 wt% SBS content GF-WTB/SBS composite-modified binders under $-24\text{ }^{\circ}\text{C}$, low-temperature crack resistance evaluation index k-value increased by 15.7% from 0 to 4 wt% GF-WTB dosage. Addition of GF-WTB can elevate the low-temperature crack resistance of SBS-modified asphalt.
- (3) In comprehensively considering the high-temperature PG, high-temperature sensitivity, k-value increasing rate, and GF-WTB dosage, 4 wt% SBS content with 2 wt% GF-WTB as a secondary modifier is the optimal combination.
- (4) FTIR, SEM, and EDS microscopic tests analysis shows that the GF-WTB successfully grafted by UP152 coupling agent is of thicker and rougher surface and a vinyl functional group was introduced, improving the adhesion of the GF-WTB to the SBS-modified asphalt. Silane coupling agent modification pretreatment for GF-WTB is one important and indispensable step for GF-WTB/SBS composite-modified binder preparation.
- (5) AFM observation found that SBS and GF-WTB exist in GF-WTB/SBS composite-modified asphalt in their own specific structural forms and the two modifiers have good compatibility. This compound form can better absorb asphalt light components, improve the elasticity and toughness of asphalt, and then improve high- and low-temperature properties of asphalt.

The good asphalt properties will transmit to the pavement performance in each respective asphalt mixture. GF-WTB/SBS composite-modified asphalt anti-aging performance and its mixture pavement performance will be further researched.

Author Contributions: Conceptualization, Y.N. and Q.L.; methodology, Z.X.; software, Q.L. and S.Z.; validation, X.H.; formal analysis, Q.L. and Z.X.; investigation, S.Z. and X.H.; resources, Y.N.; data curation, Y.N.; writing—original draft preparation, Q.L., Z.X. and S.Z.; writing—review and editing, Y.N., Q.L. and X.H.; visualization, Z.X.; supervision, Y.N.; project administration, Y.N.; funding acquisition, Y.N. All authors have read and agreed to the published version of the manuscript.

Funding: This research was funded by the Hunan Provincial Natural Science Foundation of China, grant number 2022JJ30259.

Institutional Review Board Statement: Not applicable.

Informed Consent Statement: Not applicable.

Data Availability Statement: The data used to support the findings of this study are available from the corresponding authors upon reasonable request.

Conflicts of Interest: The authors declare no conflict of interest.

References

1. Beauson, J.; Laurent, A.; Rudolph, D.P.; Jensen, J.P. The complex end-of-life of wind turbine blades: A review of the European context. *Renew. Sust. Energy Rev.* **2022**, *155*, 111847. [\[CrossRef\]](#)
2. Liu, P.; Barlow, C.Y. Wind turbine blade waste in 2050. *Waste Manag.* **2017**, *62*, 229–240. [\[CrossRef\]](#) [\[PubMed\]](#)
3. Chen, J.L.; Wang, J.H.; Ni, A.Q. Recycling and reuse of composite materials for wind turbine blades: An overview. *J. Reinf. Plast. Comp.* **2019**, *12*, 567–577. [\[CrossRef\]](#)
4. Alshannaq, A.A.; Bank, L.C.; Scott, D.W.; Gentry, R. A decommissioned wind blade as a second-life construction material for a transmission pole. *Constr. Mater.* **2021**, *1*, 95–104. [\[CrossRef\]](#)
5. Mishnaevsky, L.; Branner, K.; Petersen, H.N.; Beauson, J.; McGugan, M.; Sørensen, B.F. Materials for wind turbine blades: An overview. *Materials* **2017**, *10*, 1285. [\[CrossRef\]](#)
6. Beauson, J.; Lilholt, H.; Brondsted, P. Recycling solid residues recovered from glass fibre-reinforced composites—a review applied to wind turbine blade materials. *J. Reinf. Plast. Comp.* **2014**, *33*, 1542–1556. [\[CrossRef\]](#)
7. Pickering, S.J. Recycling technologies for thermoset composites—current status. *Comp. A* **2006**, *37*, 1206–1215. [\[CrossRef\]](#)
8. Pimenta, S.; Pinho, S.T. Recycling carbon fibre reinforced polymers for structural applications: Technology review and market outlook. *Waste Manag.* **2011**, *31*, 378–392. [\[CrossRef\]](#)
9. Meira-Castro, A.C.; Carvalho, J.P.; Ribeiro, M.C.S.; Meixedo, J.P.; Silva, F.J.G.; Fiúza, A.; Dinis, M.L. An integrated recycling approach for GFRP pultrusion wastes: Recycling and reuse assessment into new composite materials using Fuzzy Boolean Nets. *J. Clean. Prod.* **2014**, *66*, 420–430. [\[CrossRef\]](#)
10. Paulsen, E.B.; Enevoldsen, P.A. Multidisciplinary review of recycling methods for end-of-life wind turbine blades. *Energies* **2021**, *14*, 4247. [\[CrossRef\]](#)
11. Asokan, P.; Osmani, M.; Price, A.D.F. Assessing the recycling potential of glass fibre reinforced plastic waste in concrete and cement composites. *J. Clean. Prod.* **2009**, *17*, 821–829. [\[CrossRef\]](#)
12. Ribeiro, M.C.S.; Meira-Castro, A.C.; Silva, F.G.; Santos, J.; Meixedo, J.P.; Fiúza, A.; Dinis, M.L.; Alvim, M.R. Re-use assessment of thermoset composite wastes as aggregate and filler replacement for concrete-polymer composite materials: A case study regarding GFRP pultrusion wastes. *Resour. Conserv. Recycl.* **2015**, *104*, 417–426. [\[CrossRef\]](#)
13. Schmidl, E.; Hinrichs, S. Geocycle provides sustainable recycling of rotor blades in cement plant. *DEWI Mag.* **2010**, *36*, 6–14.
14. Zhu, H.Z.; Tan, Q.Q.; Yang, X.S.; Fan, S.P.; Zhao, H.D. Research status and prospect of fiber modified asphalt mixture performance. *Sci. Technol. Eng.* **2022**, *22*, 2573–2584.
15. Liu, H. Study on the Evaluation of Performance of the Regenerated Fiber Reinforced Asphalt Pavements. Master's Thesis, Beijing Jiaotong University, Beijing, China, 2011.
16. Dehghan, Z.; Modarres, A. Evaluating the fatigue properties of hot mix asphalt reinforced by recycled PET fibers using 4-point bending test. *Constr. Build. Mater.* **2017**, *139*, 384–393. [\[CrossRef\]](#)
17. Yang, Q.L.; Hong, B.; Lin, J.; Wang, D.W.; Zhong, J.; Oeser, M. Study on the reinforcement effect and the underlying mechanisms of a bitumen reinforced with recycled glass fiber chips. *J. Clean. Prod.* **2019**, *251*, 119768. [\[CrossRef\]](#)
18. Zhang, Y.; Huang, Y.; Liu, L.; Wu, L.N. Surface modification of aramid fiber with γ -ray radiation for improving interfacial bonding strength with epoxy resin. *J. Appl. Polym. Sci.* **2007**, *106*, 2251–2262. [\[CrossRef\]](#)
19. Gao, J.; Dai, Y.Y.; Wang, X.; Huang, J.Y.; Yao, J.; Yang, J.; Liu, X.Y. Effects of different fluorination routes on aramid fiber surface structures and interlaminar shear strength of its composites. *Appl. Surf. Sci.* **2013**, *270*, 627–633. [\[CrossRef\]](#)
20. Kim, J.G.; Choi, I.; Lee, D.G.; Seo, I.S. Flame and silane treatments for improving the adhesive bonding characteristics of aramid/epoxy composites. *Compos. Struct.* **2011**, *93*, 2696–2705. [\[CrossRef\]](#)
21. Ai, T.; Wang, R.; Zhou, W. Effect of grafting alkoxysilane on the surface properties of Kevlar fiber. *Polym. Composite.* **2007**, *28*, 412–416. [\[CrossRef\]](#)
22. Liu, J.L.; Xie, X.F.; Li, L.F. Experimental study on mechanical properties and durability of grafted nano-SiO₂ modified rice straw fiber reinforced concrete. *Constr. Build. Mater.* **2022**, *347*, 128575. [\[CrossRef\]](#)
23. Lei, L.L.; Wang, Q.; Xu, S.S.; Wang, N.; Zheng, X. Fabrication of superhydrophobic concrete used in marine environment with anti-corrosion and stable mechanical properties. *Constr. Build. Mater.* **2020**, *251*, 118946. [\[CrossRef\]](#)
24. Wang, X.P.; Hong, L.; Wu, H.J.; Liu, H.L.; Jia, D.M. Grafting waste rubber powder and its application in asphalt. *Constr. Build. Mater.* **2021**, *271*, 121881. [\[CrossRef\]](#)
25. JT/T 533-2020; Fiber for Asphalt Pavements. China Communications Press: Beijing, China, 2020.
26. JTG E20-2011; Standard Test Methods of Bitumen and Bituminous Mixtures for Highway Engineering. China Communications Press: Beijing, China, 2011.
27. Premkumar, L.; Chehab, G.; Solaimanian, M. Evaluation of low-temperature properties of asphalt binders and mixtures. *Transport. Res. Rec.* **2013**, *2370*, 102–108. [\[CrossRef\]](#)
28. AASHTO T313-12; Standard Method of Test for Determining the Flexural Creep Stiffness of ASPHALT binder Using the Bending Beam Rheometer (BBR). AASHTO: Washington, DC, USA, 2016.
29. Azarhoosh, A.; Koohmishi, M. Investigation of the rutting potential of asphalt binder and mixture modified by styrene-ethylene/propylene-styrene nanocomposite. *Constr. Build. Mater.* **2020**, *255*, 119363. [\[CrossRef\]](#)
30. Xu, J.Q.; Yang, E.H.; Wang, S.F.; Li, S.J. Study on low temperature performance evaluation indicator of sasobit warm mix asphalt. *J. Highw. Transp. Res. Dev.* **2020**, *37*, 8–14.

31. Tan, Y.Q.; Fu, Y.K.; Ji, L.; Zhang, L. Low-temperature evaluation index of rubber asphalt. *J. Harbin Inst. Technol.* **2016**, *48*, 66–70.
32. Nie, Y.H.; Sun, S.H.; Ou, Y.J.; Zhou, C.Y.; Mao, K.L. Experimental investigation on asphalt binders ageing behavior and rejuvenating feasibility in multicycle repeated ageing and recycling. *Adv. Mater. Sci. Eng.* **2018**, *2018*, 5129260. [[CrossRef](#)]
33. Nie, Y.H.; Gao, W.J.; Zhou, C.Y.; Yu, P.H.; Song, X.J. Evaluation of ageing behaviors of asphalt binders using FTIR tests. *Int. J. Pavement Res. Technol.* **2021**, *14*, 615–624. [[CrossRef](#)]
34. Loeber, L.; Sutton, O.; Morel, J.; Muller, G. New direct observations of asphalts and asphalt binder by scanning electron microscopy and atomic force microscopy. *J. Microsc.* **1996**, *182*, 32–39. [[CrossRef](#)]

Disclaimer/Publisher’s Note: The statements, opinions and data contained in all publications are solely those of the individual author(s) and contributor(s) and not of MDPI and/or the editor(s). MDPI and/or the editor(s) disclaim responsibility for any injury to people or property resulting from any ideas, methods, instructions or products referred to in the content.